Polyhedron 108 (2016) 131–142

Contents lists available at ScienceDirect

Polyhedron

journal homepage: www.elsevier.com/locate/poly

Cyanate groups in higher oxidation state metal cluster chemistry: Mixed-valence (II/III) Mn_{16} and Mn_{18} clusters

Dimitris I. Alexandropoulos [a], Eleni E. Moushi [b], Constantina Papatriantafyllopoulou [b,c], Christine M. Beavers [d], Simon J. Teat [d], Anastasios J. Tasiopoulos [b], George Christou [c], Theocharis C. Stamatatos [a,*]

[a] Department of Chemistry, Brock University, St. Catharines, Ontario L2S 3A1, Canada
[b] Department of Chemistry, University of Cyprus, 1678 Nicosia, Cyprus
[c] Department of Chemistry, University of Florida, Gainesville, FL 32611-7200, USA
[d] Advanced Light Source, Lawrence Berkeley National Laboratory, 1 Cyclotron Road, Berkeley, CA 94720, USA

ARTICLE INFO

Article history:
Received 19 August 2015
Accepted 18 November 2015
Available online 2 December 2015

Keywords:
Manganese
Cyanates
2-(Hydroxymethyl)pyridine
Crystal structures
Magnetism

ABSTRACT

The employment of cyanato (OCN^-) group in high oxidation state manganese cluster chemistry, in conjunction with carboxylate ions and the organic chelating/bridging ligand 2-(hydroxymethyl)pyridine (hmpH), is reported. The syntheses, crystal structures, and magnetochemical characterization are described for $[Mn_{16}O_8(OR)_4(OCN)_4(O_2CMe)_{12}(hmp)_6(ROH)_2]$ (R = Me (**1**), Et (**2**)) and $[Mn_{18}O_{14}(O_2CR)_{18}(hmp)_4(hmpH)_2(H_2O)_2]$ (R = Me (**3**), Et (**4**)). The 2:1:1:1 reactions of $Mn(O_2CMe)_2{\cdot}4H_2O$, hmpH, NaOCN and NEt_3 in solvent MeOH or EtOH afford the isostructural complexes $[Mn_{16}O_8(OR)_4(OCN)_4(O_2CMe)_{12}(hmp)_6(ROH)_2]$ (R = Me (**1**), Et (**2**)). The $[Mn_{16}(\mu_4\text{-}O)_4(\mu_3\text{-}O)_4(\mu\text{-}OMe)_4(\mu_3\text{-}OR)_6(\mu\text{-}OR)_6]^{10+}$ core of representative complex **1** comprises a $Mn^{II}_4Mn^{III}_4$ double-cubane subunit attached on either side to two symmetry-related $Mn^{II}Mn^{III}_3$ defective dicubanes. A similar reaction of $Mn(O_2CR)_2{\cdot}4H_2O$, hmpH, NaOCN and NEt_3, but in solvent MeCN, led instead to the formation of $[Mn_{18}O_{14}(O_2CR)_{18}(hmp)_4(hmpH)_2(H_2O)_2]$ (R = Me (**3**), Et (**4**)). Compounds **3** and **4** are very similar to each other and can be described as a central $[Mn^{III}_4(\mu\text{-}O)_6]$ rodlike subunit attached on either side to two symmetry-related $[Mn_7O_9]$ subunits. Variable-temperature, solid-state dc and ac magnetic susceptibility studies revealed the presence of predominant antiferromagnetic exchange interactions in all compounds, and possible $S = 2$ or 1 (for **1** and **2**) and $S = 0$ (for **3** and **4**) ground state spin values. The combined results demonstrate the ability of cyanato groups to facilitate the formation of new polynuclear $Mn^{II/III}$ complexes with structures different than these obtained from the use of the related azides.

1. Introduction

The synthesis and characterization of new polynuclear Mn complexes have been of great interest over the last three decades, or so, due to their relevance to bioinorganic chemistry and single-molecule magnetism. In the former area, bioinorganic chemists focus on the preparation of synthetic models for the structure, spectroscopic properties and/or function of the active sites of several Mn redox enzymes, the most fascinating of which is the water-oxidizing complex (WOC) of green plants and cyanobacteria, which is a Mn_4Ca species [1]. From a magnetism viewpoint, manganese complexes often possess a large number of unpaired electrons and a significant magnetoanisotropy originating from the Jahn–Teller distorted Mn^{III} ions; thus, they are excellent candidates as single-molecule magnets (SMMs) [2]. Transition metal-based SMMs are individual molecules that have a significant energy barrier to magnetization relaxation, and the upper limit to the barrier (U) is given by $S^2|D|$ or $(S^2 - 1/4)|D|$ for integer and half-integer spin systems, respectively, where D is the zero-field splitting parameter [3]. Hence, SMMs represent a molecular route to nanoscale magnetism, with potential applications in information storage [4] and spintronics [5] at the molecular level, and use as quantum bits in quantum computation [6].

Azido (N_3^-) ligand has been known for years as one of the most flexible, multitopic and versatile groups in coordination chemistry, capable of bridging many metal centers and yielding beautiful structures with interesting magnetic properties [7]. It is now established that end-on (EO) bridging azides can promote strong ferromagnetic exchange interactions between the metal spin carriers,

* Corresponding author. Tel.: +1 905 688 5550; fax: +1 905 682 9020.
E-mail address: tstamatatos@brocku.ca (T.C. Stamatatos).

http://dx.doi.org/10.1016/j.poly.2015.11.031
0277-5387/

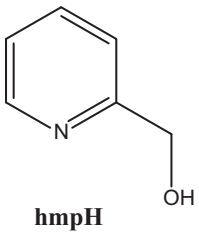

hmpH

Scheme 1. The organic ligand 2-(hydroxymethyl)pyridine (hmpH) discussed in the text.

thus leading to high-spin molecules and/or SMMs [8]. The employment of azido groups in Mn cluster chemistry, in combination with additional organic chelates (i.e., pyridyl alcohols, diols and triols), has led to a large number of Mn^{III}-containing compounds with nuclearities of up to $\{Mn_{26}\}$ [9] and *S* values as large as 83/2 [10], 74/2 [11], and 51/2 [12].

We have recently turned our attention into the employment of cyanates as bridging ligands and ferromagnetic couplers in Mn^{III} cluster chemistry. Cyanato groups (OCN^-), as well as azides, belong to the general class of pseudohalides and their use in divalent metal cluster chemistry has been extensively investigated. In the most of the cases, however, cyanates have been employed in M^{2+}-chemistry for magnetostructural correlations in structurally similar M^{2+}/N_3^- and M^{2+}/OCN^- complexes [13–15]. In contrast to the relatively extensive use of cyanates in divalent metal chemistry, there appears to be a missing gap in higher oxidation state metal chemistry, and particularly in Mn^{III} coordination chemistry. Reasons for that are probably the hypothetic structural similarities of the large in number Mn^{III}/N_3^- clusters with the corresponding Mn^{III}/OCN^- species, as well as the trivial magnetostructural correlations between the two families of complexes that might not lead to any new, significant magnetic results. However, we have shown previously that the combined use of bridging OCN^- and either pyridyl diols or pyridyl dioximes in Mn cluster chemistry can yield $Mn_{14}^{II/III}$ and $Mn_{16}^{II/III/IV}$ clusters, respectively, with different structural topologies and magnetic properties than those obtained from the corresponding reactions with azides [16].

We here report our results from the investigation of the Mn/RCO_2^-/OCN^-/hmpH (R = Me, Et) reaction system, where hmpH is 2-(hydroxymethyl)pyridine (Scheme 1), under different solvent media. The anion of hmp^- is a pyridyl alkoxide-based chelating/bridging ligand [17], and was the ligand of choice due to its ability to foster the formation of high nuclearity Mn^{III}-containing products [18] with interesting magnetic properties, such as high-spin molecules and SMMs [19]. Thus, the above general reaction system led us to the isolation and characterization of two new hexadecanuclear $[Mn_6^{II}Mn_{10}^{III}O_8(OR)_4(OCN)_4(O_2CMe)_{12}(hmp)_6(ROH)_2]$ (R = Me (**1**), Et (**2**)) and two octadecanuclear $[Mn_4^{II}Mn_{14}^{III}O_{14}(O_2CR)_{18}(hmp)_4(hmpH)_2(H_2O)_2]$ (R = Me (**3**), Et (**4**)) complexes, which are OCN^-- and solvent-dependent.

2. Experimental

2.1. General and physical measurements

All manipulations were performed under aerobic conditions using chemicals and solvents as received. $Mn(O_2CEt)_2{\cdot}4H_2O$ was prepared as described elsewhere [20].

Infrared spectra were recorded in the solid state on a Bruker's FT-IR spectrometer (ALPHA's Platinum ATR single reflection) in the 4000–450 cm^{-1} range. Elemental analyses (C, H, and N) were performed on a Perkin–Elmer 2400 Series II Analyzer. Direct current (dc) and alternating current (ac) magnetic susceptibility studies were performed at the University of Florida Chemistry Department on a Quantum Design MPMS-XL SQUID susceptometer equipped with a 7 T magnet and operating in the 1.8–400 K range. Samples were embedded in solid eicosane to prevent torquing. Alternating current magnetic susceptibility measurements were performed in an oscillating ac field of 3.5 G and a zero dc field. Oscillation frequencies were in the 50–1000 Hz range. Pascal's constants were used to estimate the diamagnetic correction, which was subtracted from the experimental susceptibility to give the molar paramagnetic susceptibility (χ_M) [21].

2.2. Compound preparation

2.2.1. $[Mn_{16}O_8(OMe)_4(OCN)_4(O_2CMe)_{12}(hmp)_6(MeOH)_2]$ (**1**)

To a stirred, colorless solution of hmpH (0.10 mL, 1.0 mmol) and NEt_3 (0.14 mL, 1.0 mmol) in MeOH (25 mL) was added solid NaOCN (0.07 g, 1.0 mmol). The resulting colorless suspension was kept under magnetic stirring at room temperature for about 10 min, followed by the consecutive addition of solid $Mn(O_2CMe)_2{\cdot}4H_2O$ (0.49 g, 2.0 mmol). The resulting dark brown suspension was stirred for a further 2 h, during which time all the solids dissolved. The solution was then filtered, and the filtrate was layered with Et_2O (50 mL). After 2 days, dark red rod-like crystals of **1** had appeared and were collected by filtration, washed with cold MeOH (2 × 5 mL) and Et_2O (2 × 5 mL), and dried in air; the yield was 50%. The crystalline solid was analyzed as solvent-free **1**. *Anal.* Calc. for $C_{70}H_{92}Mn_{16}N_{10}O_{48}$: C, 30.90; H, 3.41; N, 5.15. Found: C, 30.65; H, 3.22; N, 5.26%. Selected ATR data (cm^{-1}): 3422mb, 2200vs, 1572vs, 1484w, 1418s, 1338m, 1292w, 1156w, 1066s, 1044s, 766m, 708m, 664s, 630s, 586s, 552s.

2.2.2. $[Mn_{16}O_8(OEt)_4(OCN)_4(O_2CMe)_{12}(hmp)_6(EtOH)_2]$ (**2**)

This complex was prepared in the same manner as complex **1** but using EtOH (25 mL) as the reaction solvent. After 4 days, dark red rod-like crystals of **2** had appeared and were collected by filtration, washed with cold EtOH (2 × 5 mL) and Et_2O (2 × 5 mL), and dried in air; the yield was 40%. The crystalline solid was analyzed as solvent-free **2**: *Anal.* Calc. for $C_{76}H_{104}Mn_{16}N_{10}O_{48}$: C, 32.55; H, 3.74; N, 4.99. Found: C, 32.22; H, 3.48; N, 5.06%. Selected ATR data (cm^{-1}): 3420mb, 2198vs, 1572vs, 1482w, 1414vs, 1290w, 1156w, 1066s, 1046s, 766m, 708m, 664s, 632s, 582s, 480w.

2.2.3. $[Mn_{18}O_{14}(O_2CMe)_{18}(hmp)_4(hmpH)_2(H_2O)_2]$ (**3**)

To a stirred, colorless solution of hmpH (0.10 mL, 1.0 mmol) and NEt_3 (0.14 mL, 1.0 mmol) in MeCN (25 mL) was added solid NaOCN (0.07 g, 1.0 mmol). The resulting colorless suspension was kept under magnetic stirring at room temperature for about 10 min, followed by the consecutive addition of solid $Mn(O_2CMe)_2{\cdot}4H_2O$ (0.49 g, 2.0 mmol). The resulting dark brown suspension was stirred overnight, during which time all the solids dissolved. The solution was then filtered, and the filtrate was layered with Et_2O (50 mL). After 4 days, dark brown rod-like crystals of **3** had appeared and were collected by filtration, washed with cold MeCN (2 × 5 mL) and Et_2O (2 × 5 mL), and dried under vacuum; the yield was 30%. The crystalline solid was analyzed as solvent-free **3**: *Anal.* Calc. for $C_{72}H_{96}Mn_{18}N_6O_{58}$: C, 29.19; H, 3.27; N, 2.84. Found: C, 28.87; H, 2.92; N, 2.96%. Selected ATR data (cm^{-1}): 3446mb, 1570vs, 1414vs, 1342m, 1290w, 1156w, 1076m, 1048m, 766m, 718s, 668s, 612s, 558s, 464w, 408w.

2.2.4. $[Mn_{18}O_{14}(O_2CEt)_{18}(hmp)_4(hmpH)_2(H_2O)_2]$ (**4**)

This complex was prepared in the same manner as complex **3** but using $Mn(O_2CEt)_2{\cdot}4H_2O$ (0.55 g, 2.0 mmol) as the Mn salt. After 2 days, dark brown rod-like crystals of **4** had appeared and were collected by filtration, washed with cold MeCN (2 × 5 mL) and Et_2O (2 × 5 mL), and dried under vacuum; the yield was 43%. The

crystalline solid was analyzed as solvent-free **4**: *Anal.* Calc. for $C_{90}H_{132}Mn_{18}N_6O_{58}$: C, 33.62; H, 4.14; N, 2.61. Found: C, 33.28; H, 4.04; N, 2.88%. Selected ATR data (cm^{-1}): 3426mb, 1608vs, 1576vs, 1536vs, 1464s, 1418vs, 1372m, 1296m, 1156w, 1080m, 882w, 812w, 766w, 714m, 664m, 612s, 558m.

2.3. Single-crystal X-ray crystallography

The crystallographic data and structure refinement details for complexes **1**–**4** are summarized in Table 1. Single-crystal X-ray diffraction data for **1**, **2** and **4** were collected on an Oxford-Diffraction Supernova diffractometer, equipped with a CCD area detector utilizing Mo Ka (λ = 0.71073) (for **1** and **2**) and Cu Kα (λ = 1.5418 Å) radiation (for **4**). Suitable crystals were attached to glass fibers using paratone-N oil and transferred to a goniostat where they were cooled for data collection. Empirical absorption corrections (multiscan based on symmetry-related measurements) were applied using CrysAlis RED software [22]. The structures were solved by direct methods using SIR2004 [23] and refined on F^2 using full-matrix least-squares with SHELXL97 [24]. Software packages used were as follows: CrysAlis CCD for data collection [22], CrysAlis RED for cell refinement and data reduction [22], WINGX for geometric calculations [25], and DIAMOND [26] for molecular graphics. The non-H atoms were treated anisotropically, whereas the aromatic H atoms were placed in calculated, ideal positions and refined as riding on their respective carbon atoms. The H atoms of water molecules could not be located. Electron density contributions from disordered guest molecules were handled using the SQUEEZE procedure from the PLATON software suit [27]. Several restraints (DFIX, ISOR, DELU) have been applied in order to limit the disorder of the coordinated molecules in the crystal structures of complexes **1** and **2** (e.g. of the cyanate ligands (O23–C34–N4, O24–C35–N5), the methanol ligand (C2) in compound **1** and of the cyanate ligand (O21–C32–N and the ethanol ligands (C33–C34–O22, C37–C38–O24 in compound **2**).

Data for a selected crystal of **3** were collected at Station 11.3.1 of the Advanced Light Source at Lawrence Berkeley National Laboratory, using a Bruker Apex II CCD diffractometer (ω_o rotation with narrow frames, synchrotron radiation at 0.7749 Å, silicon 111 monochromator). The structure was solved by direct methods and refined using the SHELX-TL suite of programs [28]. All fully occupied non-H atoms were refined anisotropically. All disordered or partially groups were left isotropic to conserve the data to parameter ratio. In this case the refinement would require extensive restraints to produce nice looking displacement parameters and therefore it seemed more sensible just to leave them isotropic. The lattice solvate molecules did not refine well and were heavily overlapped. After trying numerous disorder models, the decision was made to use SQUEEZE. The solvents, as modeled, refined to total 2 MeCN and 0.5 Et_2O in the void over five positions in the asymmetric unit. This would yield 4 MeCN and 1 Et_2O in the whole solvent void (~130 e^-), which is reasonably close to the SQUEEZE outcome of 148 e^-. One of the ligands is disordered, with the hydroxyl oxygen atom mostly engaged in a long bond with Mn7, but 20% of the time has been rotated away from that contact. The hydrogen atom on O2 cannot be located in the difference map when it is interacting with Mn7, but a reasonable hydrogen position can be refined otherwise. The hydrogen atoms on O1W were found in the difference map and refined using a combination of similarity restraints and distance constraints. All hydrogen atoms were refined with displacement parameters riding, with U(H) = 1.5U(O) and U(H) = 1.2U(C).

3. Results and discussion

3.1. Synthetic comments and IR spectra

The Mn/N_3^-/hmpH reaction system has been extensively studied over the last ten years, yielding polynuclear Mn species with beautiful motifs, large ground state spin values, and SMM behaviors.

Table 1
Crystal and structure refinement details for complexes **1**–**4**.

Parameter	1	2	3	4
Formula[a]	$C_{70}H_{92}Mn_{16}N_{10}O_{48}$	$C_{76}H_{104}Mn_{16}N_{10}O_{48}$	$C_{72}H_{94.4}Mn_{18}N_6O_{58}$	$C_{90}H_{132}Mn_{18}N_6O_{58}$
Fw[a] (g mol^{-1})	2720.56	2804.72	2960.84	3214.94
Crystal color and type	brown polyhedral	brown rod	brown rod	brown rod
Crystal size (mm)	0.06 × 0.04 × 0.03	0.11 × 0.06 × 0.02	0.26 × 0.07 × 0.02	0.07 × 0.01 × 0.006
Crystal system	monoclinic	monoclinic	triclinic	monoclinic
Space group	$P2_1/n$	$P2_1/n$	$P\bar{1}$	$C2/c$
a (Å)	14.218(2)	14.7006(4)	14.377(3)	27.993(3)
b (Å)	14.611(2)	14.6302(4)	15.219(3)	14.9069(6)
c (Å)	26.483(3)	26.2109(6)	15.672(3)	31.1573(19)
α (°)	90	90	70.267(2)	90
β (°)	90.8721(1)	91.761(2)	76.925(3)	108.617(9)
γ (°)	90	90	82.243(3)	90
V ($Å^3$)	5500.9(1)	5634.6(3)	3137.5(10)	12321.0(16)
Z	2	2	1	4
T (K)	100.0(2)	100.0(2)	100.0(2)	100.0(2)
Radiation (Å)	0.71073 (Mo Kα)	0.71073 (Mo Kα)	0.7749 (synchrotron)	1.5418 (Cu Kα)
ρ_{calc} (g cm^{-3})	1.641	1.652	1.567	1.732
μ (mm^{-1})	1.852	1.811	1.813	15.247
θ range (°)	2.89–25.00	2.89–25.00	3.18–33.6	3.33–61.68
Index ranges	$-16 \leqslant h \leqslant 16$ $-17 \leqslant k \leqslant 17$ $-31 \leqslant l \leqslant 28$	$-12 \leqslant h \leqslant 17$ $-17 \leqslant k \leqslant 16$ $-31 \leqslant l \leqslant 31$	$-20 \leqslant h \leqslant 20$ $-21 \leqslant k \leqslant 21$ $-22 \leqslant l \leqslant 22$	$-20 \leqslant h \leqslant 31$ $-11 \leqslant k \leqslant 16$ $-35 \leqslant l \leqslant 30$
Collected reflections	9683	9920	19183	6188
Independent reflections	6056 (R_{int} = 0.0769)	7808 (R_{int} = 0.0472)	16061 (R_{int} = 0.0455)	4818 (R_{int} = 0.0348)
Final R[b,c] indices [$I > 2\sigma(I)$]	R_1 = 0.0664 wR_2 = 0.1652	R_1 = 0.0516 wR_2 = 0.1422	R_1 = 0.0388 wR_2 = 0.1029	R_1 = 0.0420 wR_2 = 0.1066
$(\Delta\rho)_{maximum,minimum}$ (e $Å^{-3}$)	1.477, −1.178	1.435, −1.339	1.441, −0.733	0.589, −0.403

[a] Lattice solvate molecules are not included.
[b] $R_1 = \Sigma(||F_o| - |F_c||)/\Sigma|F_o|$.
[c] $wR_2 = [\Sigma[w(F_o^2 - F_c^2)^2]/\Sigma[w(F_o^2)^2]]^{1/2}$, $w = 1/[\sigma^2(F_o^2) + (ap)^2 + bp]$, where $p = [\max(F_o^2, 0) + 2F_c^2]/3$.

Two representative examples are the ferromagnetic $[Mn^{II}_4Mn^{III}_6O_4(N_3)_4(hmp)_{12}]^{2+}$ cluster with $S = 22$ [19] and the $[Mn^{II}_2Mn^{III}_2(N_3)_4(hmp)_6]$ rhombus-like complex with an $S = 9$ ground state and slow magnetization relaxation [29]. On the other hand, the co-presence of azide and carboxylate groups in Mn/hmpH chemistry has not yet led to any crystalline material. Recently, we have started a program aiming at the use of heteroatomic-type pseudohalides, such as OCN^-, as structure-directing ligands and ferromagnetic couplers in Mn^{III} cluster chemistry. We have now extended our studies to incorporate cyanates in Mn carboxylate chemistry, in conjunction with various chelates, such as the anion of hmp^-.

A variety of reactions differing in the cyanate amount, the Mn:hmpH ratio, the carboxylate groups present, the organic base, and the reaction solvent(s) were explored in identifying the following successful systems. The one-pot reaction of $Mn(O_2CMe)_2{\cdot}4H_2O$ with hmpH in a 2:1 molar ratio in solvent MeOH or EtOH, in the presence of one equivalent of each NaOCN and NEt_3, gave a brown solution that, upon filtration and layering with Et_2O, afforded dark red crystals of the complexes $[Mn_{16}O_8(OR)_4(OCN)_4(O_2CMe)_{12}(hmp)_6(ROH)_2]$ ($Mn^{II}_6Mn^{III}_{10}$; R = Me (**1**), Et (**2**)) in yields of 50% and 40%, respectively. The general formation of **1** and **2** is summarized in Eq. (1).

$$16Mn^{2+} + 12MeCO_2^- + 6hmpH + 4NCO^- + 16NEt_3 + 6ROH + \frac{5}{2}O_2 + 3H_2O \rightarrow [Mn_{16}O_8(OR)_4(OCN)_4(O_2CMe)_{12}(hmp)_6(ROH)_2] + 16NHEt_3^+ \quad (R = Me \text{ or } Et) \qquad (1)$$

The synthesis involves Mn oxidation, undoubtedly by O_2 under the prevailing basic conditions, and Eq. (1) has been balanced accordingly. The NEt_3 reagent is essential to ensure basic conditions, and to act as a proton acceptor to facilitate the deprotonation of the hmpH groups. In addition, the presence of NEt_3 promotes the in situ generation of RO^- and O^{2-} ions through the deprotonation of ROH solvate molecules and H_2O-containing starting materials, respectively. A similar role could also be carried out by the $MeCO_2^-$ ions, but in the absence of NEt_3 longer reaction times (>24 h) are required to get a significant dark brown coloration, and the yields of isolated **1** and **2** are much lower (<10%). Employment of different organic bases, such as NMe_3, NBu^n_3 and Me_4NOH, did not afford crystalline materials but only oily products that we were not able to further characterize. A significant increase in the amount of hmpH led to yellow or pale-orange solutions indicative of Mn^{II} products. Finally, substitution of $MeCO_2^-$ ions in the Mn$(O_2CMe)_2$ precursor by other carboxylate groups, such as $EtCO_2^-$ or $Bu^tCO_2^-$, did not lead us to any crystalline material under the given reaction conditions.

Within the concept of chemical reactivity on cluster compounds, an important synthetic factor that is worthy investigating is the effect of the reaction solvent on the structural identity of the complexes. The volatility, polarity, rigidity and coordination affinity of reaction solvents are some of the features which could in principle affect the identity of a species [30]. In our case, the solvent ROH (R = Me or Et) seems to be essential for the formation of **1** and **2** because it does not only ensure the solubility of all reagents but it also serves to provide bridging RO^- groups (*vide infra*). Using nonpolar solvents, such as CH_2Cl_2 and $CHCl_3$, much longer reaction times were required and only insoluble amorphous precipitates were observed. Finally, a similar reaction with that of **1**, but in solvent MeCN instead of MeOH, gave dark brown crystals of a new octadecanuclear compound $[Mn_{18}O_{14}(O_2CMe)_{18}(hmp)_4(hmpH)_2(H_2O)_2]$ ($Mn^{II}_4Mn^{III}_{14}$; **3**) in ~30% yield. Under the same reaction conditions, the replacement of $Mn(O_2CMe)_2{\cdot}4H_2O$ by Mn$(O_2CEt)_2{\cdot}4H_2O$ led to the isolation of the similar compound $[Mn_{18}O_{14}(O_2CEt)_{18}(hmp)_4(hmpH)_2(H_2O)_2]$ ($Mn^{II}_4Mn^{III}_{14}$; **4**) in ~43% yield. The general formation of **3** and **4** is summarized in Eq. (2).

$$18Mn^{2+} + 18RCO_2^- + 6hmpH + 18NEt_3 + \frac{7}{2}O_2 + 9H_2O \rightarrow [Mn_{18}O_{14}(O_2CR)18(hmp)_4(hmpH)_2(H_2O)_2] + 18NHEt_3^+ \quad (R = Me \text{ or } Et) \qquad (2)$$

The reaction is again an oxidation by atmospheric O_2 under the prevailing basic conditions. Once the identities of **3** and **4** were established by single-crystal X-ray diffraction studies (*vide infra*), we managed to optimize the synthetic conditions and increase the isolated yields of the crystalline compounds. Note that OCN^- ions are not present in the structures of **3** and **4**, although they were added to the reaction mixtures as NaOCN. To that end, we performed the same reactions that gave **3** and **4** in the absence of NaOCN, and we were able to isolate the same products in 50% and 60% yields, respectively. These reactions suggest that there is "competition" in solution between the cyanato and carboxylate groups for the coordination with the metal ions, with carboxylate ions showing a better coordination and bridging affinity for $Mn^{II/III}$ atoms than cyanates for this particular reaction system.

In the IR spectra of complexes **1**–**4** several bands appear in the ~1595–1380 cm^{-1} range, assigned to contributions from the stretching vibrations of the aromatic ring of hmpH/hmp^- ligands, which overlap with stretches of the carboxylate bands. Thus, they do not represent pure vibrations and render exact assignments and application of the spectroscopic criterion of Deacon and Phillips [31] difficult. The IR spectra of complexes **1** and **2** exhibit a strong band at 2200 cm^{-1} and 2198 cm^{-1}, respectively. These bands are assigned to stretching vibrations of terminally bound cyanato groups through the oxygen donor atoms [32].

3.2. Description of structures

A partially labeled representation of complex **1** is shown in Fig. 1. Selected interatomic distances and angles are listed in Table 2.

Complex **1** crystallizes in the monoclinic space group $P2_1/n$ with the $[Mn_{16}O_8(OMe)_4(OCN)_4(O_2CMe)_{12}(hmp)_6(MeOH)_2]$ molecule on a special position. The centrosymmetric cluster comprises a $[Mn_{16}(\mu_4\text{-}O)_4(\mu_3\text{-}O)_4(\mu\text{-}OMe)_4(\mu_3\text{-}OR)_6(\mu\text{-}OR)_6]^{10+}$ core (Fig. 2, top) which can be conveniently dissected into three units: a central $[Mn^{II}_4Mn^{III}_4(\mu_4\text{-}O)_2(\mu_3\text{-}O)_2(\mu\text{-}O)_2(\mu_3\text{-}OR)_4]^{4+}$ and two symmetry-related $Mn^{II}Mn^{III}_3$ tetranuclear subunits (Fig. 2, bottom). The central Mn^{II}_4-Mn^{III}_4 unit consists of two $[Mn^{II}_2Mn^{III}_2(\mu_3\text{-}O)_2(\mu_3\text{-}OR)_2]^{4+}$ cubanes (Mn4′, Mn6, Mn7, Mn8, O3, O4′, O6, O7, and their symmetry-related partners), which are linked together through the μ_3-O^{2-} atoms, O4 and O4′; thus, the latter become μ_4-bridging. A tetranuclear $[Mn^{II}$-$Mn^{III}_3(\mu_3\text{-}O)(\mu_3\text{-}OR)(\mu\text{-}OR)_4]^{4+}$ subunit is attached on each side of the central $Mn^{II}_4Mn^{III}_4$ unit. The four metal ions of each $Mn^{II}Mn^{III}_3$ unit are located at the four vertices of a distorted defective dicubane, i.e., two cubanes sharing a face (Mn2, O1, Mn3, O5, and their symmetry-related partners) and each missing one metal vertex. The central $Mn^{II}_4Mn^{III}_4$ core is connected to the two extrinsic $Mn^{II}Mn^{III}_3$ units via the atoms O3, O2, O17, and their symmetric counterparts, which are thus becoming μ_4, μ_3, and μ, respectively. Hence, the metal centers are bridged in total by four μ_4-O^{2-} (O3, O4, O3′, O4′) and four μ_3-O^{2-} (O1, O2, O1′, O2′) ions, while additional linkage is provided by the alkoxido arms of the six hmp^- groups. The latter are all of the $\eta^1{:}\eta^3{:}\mu_3$ type (Fig. 3), emphasizing the bridging flexibility of this ligand, as well as its ability to bridge metal ions at different oxidation states ($Mn^{II/III}$). Peripheral ligation about the complete core is provided by six $\eta^1{:}\eta^2{:}\mu_3$ and six $\eta^1{:}\eta^1{:}\mu$ acetate groups (Fig. 3), as well as four μ-OMe^- groups, two terminal MeOH molecules (at Mn8 and Mn8′) and four terminal OCN^- ions binding through their O atom (at Mn1, Mn7, Mn1′ and Mn7′).

Charge balance considerations and an inspection of the metric parameters indicate a $6Mn^{II}$, $10Mn^{III}$ description for **1**. This was

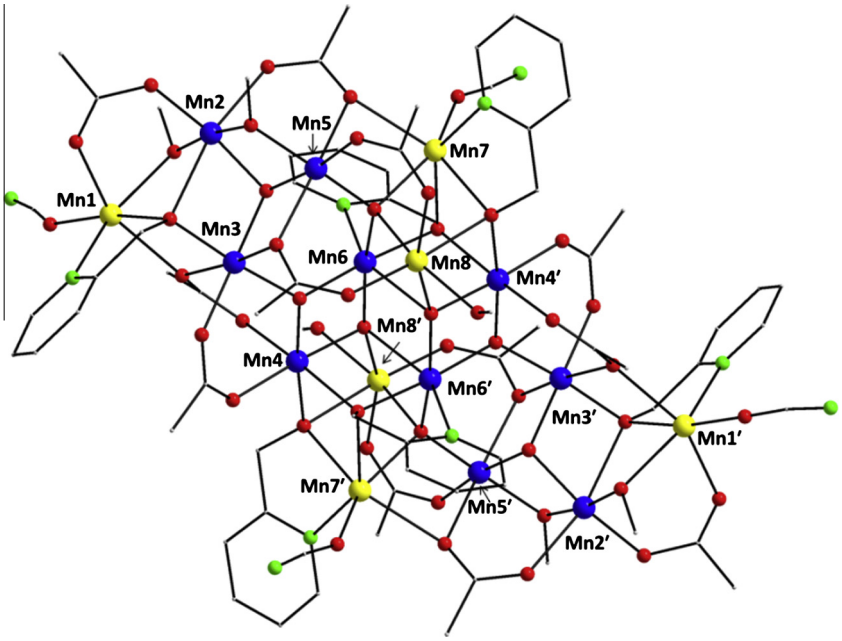

Fig. 1. Partially labeled PovRay representation of complex **1**. H atoms have been omitted for clarity. Color scheme: Mn^{II} yellow; Mn^{III} blue; O red; N green; C gray. Symmetry operation for the primed atoms in **1**: $1-x, 1-y, 2-z$. (Color online.)

Table 2
Selected interatomic distances (Å) and angles (°) for complex **1**.[a]

Bond lengths			
Mn(1)–O(23)	2.052(8)	Mn(5)–O(3)	1.845(5)
Mn(1)–O(5)	2.200(5)	Mn(5)–O(1)	1.900(4)
Mn(1)–O(20)	2.202(5)	Mn(5)–O(21)	1.922(5)
Mn(1)–O(8)	2.205(5)	Mn(5)–O(18)	1.947(5)
Mn(1)–N(1)	2.298(7)	Mn(5)–O(17)	2.225(5)
Mn(1)–O(10)	2.311(5)	Mn(5)–O(14)	2.300(5)
Mn(2)–O(20)	1.874(5)	Mn(6)–O(4)	1.911(5)
Mn(2)–O(1)	1.903(5)	Mn(6)–O(2)	1.920(4)
Mn(2)–O(9)	1.917(5)	Mn(6)–O(3)	1.939(5)
Mn(2)–O(21)	1.922(5)	Mn(6)–O(6)	1.996(4)
Mn(2)–O(16)	2.222(5)	Mn(6)–N(2)	2.308(6)
Mn(2)–O(5)	2.360(5)	Mn(6)–O(4′)	2.325(4)
Mn(3)–O(2)	1.856(4)	Mn(7)–O(24)	2.106(8)
Mn(3)–O(5)	1.904(4)	Mn(7)–O(3)	2.167(4)
Mn(3)–O(1)	1.912(5)	Mn(7)–N(3)	2.211(6)
Mn(3)–O(12)	2.004(5)	Mn(7)–O(6)	2.272(5)
Mn(3)–O(10)	2.250(5)	Mn(7)–O(7)	2.281(5)
Mn(3)–O(14)	2.270(5)	Mn(7)–O(17)	2.401(5)
Mn(4)–O(2)	1.863(4)	Mn(8)–O(19)	2.138(5)
Mn(4)–O(4)	1.918(4)	Mn(8)–O(3)	2.140(5)
Mn(4)–O(7′)	1.951(5)	Mn(8)–O(4′)	2.142(5)
Mn(4)–O(13)	2.019(5)	Mn(8)–O(15)	2.146(5)
Mn(4)–O(11)	2.165(5)	Mn(8)–O(22)	2.151(5)
Mn(4)–O(6′)	2.194(5)	Mn(8)–O(7)	2.401(5)
Bond angles			
Mn(2)–O(1)–Mn(3)	108.7(2)	Mn(6)–O(4)–Mn(8′)	159.9(2)
Mn(2)–O(1)–Mn(5)	96.7(2)	Mn(4)–O(4)–Mn(6′)	97.6(2)
Mn(3)–O(1)–Mn(5)	107.7(2)	Mn(1)–O(5)–Mn(2)	89.1(2)
Mn(3)–O(2)–Mn(4)	122.0(2)	Mn(1)–O(5)–Mn(3)	108.5(2)
Mn(3)–O(2)–Mn(6)	125.7(2)	Mn(2)–O(5)–Mn(3)	92.7(2)
Mn(4)–O(2)–Mn(6)	98.5(2)	Mn(6)–O(6)–Mn(7)	95.7(2)
Mn(5)–O(3)–Mn(6)	124.2(2)	Mn(6)–O(6)–Mn(4′)	99.6(1)
Mn(5)–O(3)–Mn(7)	108.7(2)	Mn(7)–O(6)–Mn(4′)	98.7(2)
Mn(6)–O(3)–Mn(8)	102.1(2)	Mn(7)–O(7)–Mn(8)	96.5(2)
Mn(7)–O(3)–Mn(8)	108.4(2)	Mn(7)–O(7)–Mn(4′)	106.1(2)
Mn(5)–O(3)–Mn(8)	111.4(2)	Mn(8)–O(6)–Mn(4′)	159.9(2)
Mn(6)–O(3)–Mn(7)	100.9(2)	Mn(1)–O(10)–Mn(3)	94.0(2)
Mn(4)–O(4)–Mn(6)	97.0(2)	Mn(3)–O(14)–Mn(5)	84.7(2)
Mn(4)–O(4)–Mn(8′)	101.1(2)	Mn(5)–O(17)–Mn(7)	89.7(2)
Mn(6)–O(4)–Mn(6′)	96.0(2)	Mn(1)–O(20)–Mn(2)	103.2(2)
Mn(6′)–O(4)–Mn(8′)	90.5(2)	Mn(2)–O(21)–Mn(5)	95.4(3)

[a] Symmetry code: ′ = $1-x, 1-y, 2-z$.

confirmed quantitatively by bond valence sum (BVS) [33] calculations (Table 3), which identified Mn1, Mn7, Mn8, Mn1′, Mn7′ and Mn8′ as the Mn^{II} ions, and the others as Mn^{III}. The latter was also consistent with the Jahn–Teller (JT) distortion observed in Mn^{III} ions, as expected for high-spin, d^4 ions in near-octahedral geometry, taking the form of axial elongation of the two *trans* Mn–O and/or Mn–N bonds. All Mn^{II} ions are also six-coordinate with distorted octahedral geometries. The protonation level of O^{2-} groups was also confirmed by BVS calculations (Table 3). Complex **1** does not form any significant intermolecular interactions of any kind. Further, the space-filling representation of compound **1** reveals its large nanometer-sized structure and its 'ellipsoidal' motif with average distances of ~2.1 nm (across the molecule), ~1.9 nm (perpendicular to the molecule) and ~1.4 nm (in the third dimension), as defined by the longest H···H distances (Fig. 4).

Complex **2** is almost isostructural with **1** and thus will not be further discussed. The main differences between **2** and **1** are: (i) the replacement of four bridging μ-OMe^- ions by four μ-OEt^- groups, and (ii) the presence of four terminal EtOH molecules in place of four MeOH groups in **1**. Again, BVS calculations, charge balance considerations, and inspection of metric parameters confirm a $6Mn^{II}$, $10Mn^{III}$ description for complex **2**.

Complexes **3** and **4** are very similar, and mainly differ from each other on the carboxylate ions present, i.e., $MeCO_2^-$ vs $EtCO_2^-$, respectively. As a representative example of this family of octadecanuclear clusters, complex **4** will be discussed in detail. A partially labeled representation of complex **4** is shown in Fig. 5. Selected interatomic distances and angles are listed in Table 4.

Complex **4** crystallizes in the monoclinic space group *C*2/*c* with the $[Mn_{18}O_{14}(O_2CEt)_{18}(hmp)_4(hmpH)_2(H_2O)_2]$ molecule on a special position (crystallographic inversion center). The compound can be described as a disc of ten nearly planar metal ions, with the remaining eight metals (Mn2, Mn3, Mn5, Mn9, and their symmetry-related partners) lying above and below the Mn_{10} plane. It comprises a $[Mn_{18}(\mu_4\text{-}O)_4(\mu_3\text{-}O)_{10}(\mu_3\text{-}OR)_2(\mu\text{-}OR)_8]^{12+}$ core (Fig. 6), which can be described as a central $[Mn^{III}_4(\mu\text{-}O)_6]$ rodlike subunit (Mn7, Mn8, Mn7′, Mn8′, O5, O6, O7, O5′, O6′, O7′) attached on either side to two symmetry-related $[Mn_7O_9]$ subunits. The link-

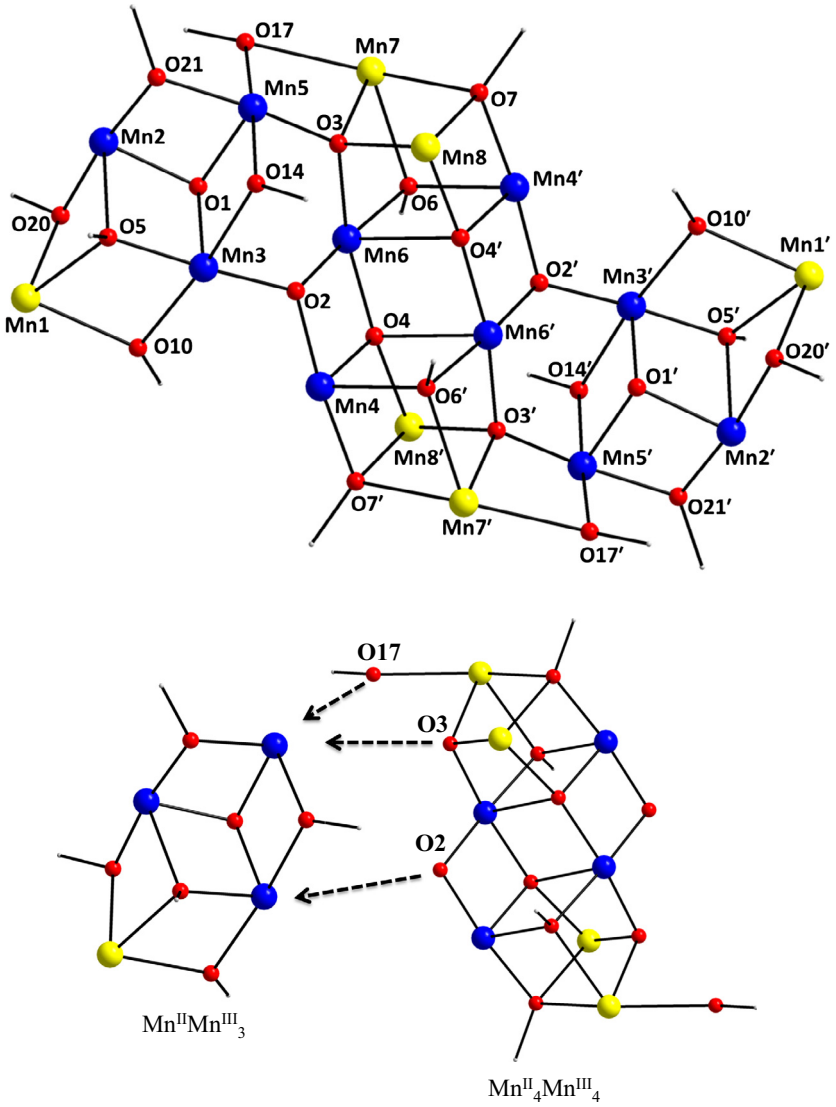

Fig. 2. Partially labeled PovRay representations of (top) the $[Mn_{16}(\mu_4\text{-}O)_4(\mu_3\text{-}O)_4(\mu\text{-}OMe)_4(\mu_3\text{-}OR)_6(\mu\text{-}OR)_6]^{10+}$ core of **1** and (bottom) the two types of constituent subunits of its core. Color scheme: same as in Fig. 1. (Color online.)

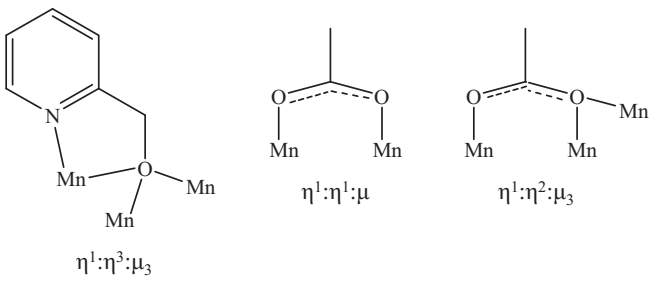

Fig. 3. The coordination modes of hmp^- and $MeCO_2^-$ ligands found in complex **1**.

age between the central unit and the two $[Mn_7O_9]$ subunits is provided by the oxido groups of the former, namely O5, O6, O7, O5′, O6′, O7′, which are thus converted from μ to μ_3. Each $[Mn_7O_9]$ subunit consists of a face-sharing set of a $[Mn_4O_4]$ cubane and two $[Mn_3O_4]$ partial cubanes. The metal centers are overall bridged by four $\mu_4\text{-}O^{2-}$ (O2, O4, O2′, O4′) and ten $\mu_3\text{-}O^{2-}$ (O1, O3, O5, O6, O7, and their symmetry related partners), while additional linkage is provided by the alkoxido arms of the six hmpH/hmp^- groups, all binding in the $\eta^1\text{:}\eta^2\text{:}\mu$ coordination mode (Fig. 7). Although rare,

Table 3
Bond valence sum (BVS)[a,b] calculations for Mn and selected O atoms in **1**.

Atom	Mn^{II}	Mn^{III}	Mn^{IV}
Mn1	1.91	1.76	1.82
Mn2	3.24	2.97	3.11
Mn3	3.19	2.92	3.06
Mn4	3.19	2.92	3.06
Mn5	3.29	3.01	3.16
Mn6	3.00	2.76	2.87
Mn7	1.80	1.66	1.71
Mn8	1.98	1.81	1.89
Atom	BVS	Assignment	
O1	1.78	O^{2-} (μ_3)	
O2	1.92	O^{2-} (μ_3)	
O3	1.90	O^{2-} (μ_4)	
O4	1.69	O^{2-} (μ_4)	

[a] The underlined value is the one closest to the charge for which it was calculated. The oxidation state is the nearest whole number to the underlined value.
[b] An O BVS in the ~1.7–2.0, ~1.0–1.2, and ~0.2–0.4 ranges is indicative of non-, single- and double-protonation, respectively.

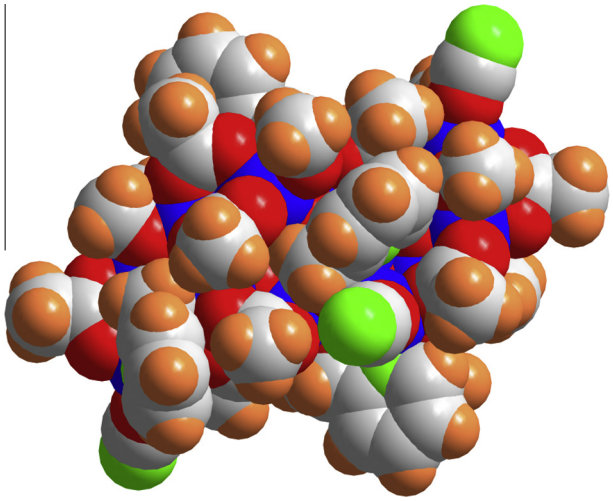

Fig. 4. Space-filling representation of **1**. Color scheme: Mn blue; O red; N green; C gray; H beige. (Color online.)

the co-presence of fully-deprotonated and neutral forms of an alkoxide-based bridging ligand, as the hmp^-/hmpH combination in **4** (and **3**), is with precedence in metal cluster chemistry [34]. Peripheral ligation about the complete core is provided by two $\eta^1{:}\eta^3{:}\mu_4$, two $\eta^1{:}\eta^2{:}\mu_3$ and fourteen $\eta^1{:}\eta^1{:}\mu$ propionate groups (Fig. 7), as well as two terminal H_2O molecules (at Mn7 and Mn7′). All Mn atoms are six-coordinate with distorted octahedral geometries.

Charge balance considerations indicate a mixed-valence Mn^{II}_4-Mn^{III}_{14} description of **4**. This was confirmed quantitatively by metric parameters and bond valence sum (BVS) calculations (Table 5), which identified Mn5, Mn5′, Mn9, and Mn9′ as the Mn^{II} ions, and the others as Mn^{III}; the latter also show Jahn–Teller (JT) distortion which takes the form of axial elongation of the *trans* Mn–O and/or Mn–N bonds. BVS calculations also confirm the protonation level of O^{2-} groups (Table 5). Complex **4** does not form any significant intermolecular interactions other than some weak C–H···π contacts between the aromatic rings of neighboring hmp^-/hmpH ligands. Further, the space-filling representation of **4** reveals its nanotubular structure with the longest H···H distance across the molecule being ~2.2 nm (Fig. 8).

In Tables 6 and 7, we have listed all the previously reported Mn clusters with nuclearities of 16 and 18, respectively, for a convenient comparison of their formulae, oxidation states description, and pertinent magnetic data such as their ground state spin (S) values and the nature of predominant magnetic exchange interactions. The combined results of Table 6 show that complexes **1** and **2** join a handful of known Mn_{16} clusters at the $Mn^{II}_6Mn^{III}_{10}$ oxidation state level, and possess a metal core topology similar, but not the same, with that reported by Christou and coworkers [45]. Further, complexes **3** and **4** are the second and third Mn_{18} clusters at the $Mn^{II}_4Mn^{III}_{14}$ oxidation level, with the $[Mn_{18}O_{14}(OMe)_{14}(O_2CBu^t)_8(MeOH)_6]$ cluster [52] being the first albeit with a completely different core topology. The same core topology with that of **3** and **4** is found in complexes $[Mn_{18}O_{14}(O_2CMe)_{18}(hep)_4(hepH)_2(H_2O)_2]^{2+}$ [51] and $[Mn_{18}O_{16}(O_2CPh)_{22}(phth)_2(H_2O)_4]^{4-}$ [53], but these have different oxidation states description, $Mn^{II}_2Mn^{III}_{16}$ and Mn^{III}_{18}, respectively.

3.3. Magnetochemistry

3.3.1. Magnetic susceptibility studies of complex *1*

Variable-temperature dc and ac magnetic susceptibility measurements were performed on powdered polycrystalline samples of **1** and **2**, restrained in eicosane to prevent torquing, in a 1 kG (0.1 T) field and in the 5.0–300 K range. The magnetic data of the two isostructural compounds are identical, and therefore only those for **1** will be discussed. The obtained data are shown as $\chi_M T$ versus T in Fig. 9.

The $\chi_M T$ product for **1** steadily decreases with decreasing temperature from 47.76 $cm^3\ mol^{-1}\ K$ at 300 K to 34.16 $cm^3\ mol^{-1}\ K$ at 100 K, and then rapidly decreases to 6.30 $cm^3\ mol^{-1}\ K$ at 5.0 K. The 300 K value is less than the spin-only ($g = 2$) value of 56.25 $cm^3\ mol^{-1}\ K$ for six Mn^{II} and ten Mn^{III} non-interacting ions, indicating the presence of predominant antiferromagnetic exchange interactions within the molecule. The 5 K value suggests a small spin ground state value of $S = 2$ or 3 for **1**; the spin-only ($g = 2$) values for $S = 2$ and 3 are 3 and 6 $cm^3\ mol^{-1}\ K$, respectively. The continuous decrease of the $\chi_M T$ product at the lowest temper-

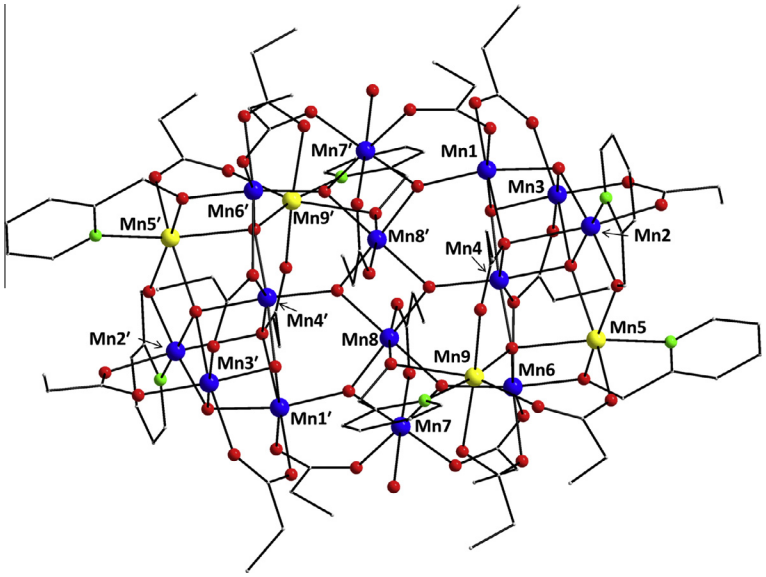

Fig. 5. Partially labeled PovRay representation of complex **4**. H atoms have been omitted for clarity. Color scheme: Mn^{II} yellow; Mn^{III} blue; O red; N green; C gray. Symmetry operation for the primed atoms in **4**: $3/2 - x, 1/2 - y, -z$. (Color online.)

Table 4
Selected interatomic distances (Å) and angles (°) for complex **4**.[a]

Bond lengths			
Mn(1)–O(3)	1.878(5)	Mn(5)–O(2)	2.200(5)
Mn(1)–O(7′)	1.892(5)	Mn(5)–N(2)	2.250(5)
Mn(1)–O(1)	1.914(5)	Mn(5)–O(4)	2.264(5)
Mn(1)–O(11)	1.965(5)	Mn(6)–O(6)	1.888(5)
Mn(1)–O(13)	2.198(4)	Mn(6)–O(9)	1.899(4)
Mn(1)–O(17)	2.345(5)	Mn(6)–O(4)	1.903(5)
Mn(2)–O(2)	1.861(4)	Mn(6)–O(25)	1.985(5)
Mn(2)–O(8)	1.904(5)	Mn(6)–O(23)	2.175(5)
Mn(2)–O(1)	1.911(5)	Mn(6)–O(20)	2.463(5)
Mn(2)–N(1)	2.020(5)	Mn(7)–O(7)	1.856(5)
Mn(2)–O(15)	2.168(5)	Mn(7)–O(6)	1.866(4)
Mn(2)–O(17)	2.421(5)	Mn(7)–O(26)	1.952(5)
Mn(3)–O(3)	1.862(4)	Mn(7)–O(12′)	1.990(4)
Mn(3)–O(1)	1.938(4)	Mn(7)–O(28)	2.217(4)
Mn(3)–O(16)	1.945(5)	Mn(7)–O(29)	2.307(4)
Mn(3)–O(19)	1.966(5)	Mn(8)–O(5)	1.899(4)
Mn(3)–O(14)	2.178(5)	Mn(8)–O(7)	1.909(4)
Mn(3)–O(2)	2.226(5)	Mn(8)–O(5′)	1.913(5)
Mn(4)–O(5)	1.867(4)	Mn(8)–O(6)	1.936(5)
Mn(4)–O(4)	1.911(4)	Mn(8)–O(27)	2.186(5)
Mn(4)–O(2)	1.933(5)	Mn(8)–O(10)	2.470(5)
Mn(4)–O(3)	1.933(5)	Mn(9)–O(4)	2.099(4)
Mn(4)–O(20)	2.222(5)	Mn(9)–O(22)	2.145(5)
Mn(4)–O(17)	2.349(2)	Mn(9)–O(18)	2.158(5)
Mn(5)–O(9)	2.106(5)	Mn(9)–O(24)	2.173(5)
Mn(5)–O(21)	2.131(5)	Mn(9)–N(3)	2.271(5)
Mn(5)–O(8)	2.166(5)	Mn(9)–O(10)	2.314(5)
Bond angles			
Mn(1)–O(1)–Mn(2)	112.8(2)	Mn(5)–O(4)–Mn(9)	113.0(2)
Mn(2)–O(1)–Mn(3)	95.1(2)	Mn(4)–O(5)–Mn(8)	128.3(2)
Mn(1)–O(1)–Mn(3)	93.7(2)	Mn(4)–O(5)–Mn(8′)	130.7(2)
Mn(2)–O(2)–Mn(4)	114.9(2)	Mn(8)–O(5)–Mn(8′)	99.1(2)
Mn(2)–O(2)–Mn(5)	99.4(2)	Mn(6)–O(6)–Mn(7)	127.1(2)
Mn(4)–O(2)–Mn(5)	98.1(2)	Mn(7)–O(6)–Mn(8)	95.44(2)
Mn(2)–O(2)–Mn(3)	87.6(2)	Mn(6)–O(6)–Mn(8)	135.6(2)
Mn(4)–O(2)–Mn(3)	89.2(2)	Mn(7)–O(7)–Mn(1′)	129.9(2)
Mn(5)–O(2)–Mn(3)	166.5(2)	Mn(7)–O(7)–Mn(8)	96.7(2)
Mn(1)–O(3)–Mn(3)	97.5(2)	Mn(8)–O(7)–Mn(1′)	133.2(2)
Mn(3)–O(3)–Mn(4)	101.0(2)	Mn(2)–O(8)–Mn(5)	99.3(2)
Mn(1)–O(3)–Mn(4)	108.4(2)	Mn(5)–O(9)–Mn(6)	105.2(2)
Mn(4)–O(4)–Mn(6)	108.0(2)	Mn(1)–O(17)–Mn(4)	82.4(2)
Mn(6)–O(4)–Mn(9)	118.7(2)	Mn(1)–O(17)–Mn(2)	83.9(1)
Mn(4)–O(4)–Mn(9)	117.6(2)	Mn(2)–O(17)–Mn(4)	84.2(1)
Mn(5)–O(4)–Mn(6)	99.3(2)	Mn(4)–O(20)–Mn(6)	82.2(2)
Mn(4)–O(4)–Mn(5)	96.7(2)		

[a] Symmetry code: ′ = 3/2 − *x*, 1/2 − *y*, −*z*.

atures may also presage an overall $S = 0$ spin ground state. Given the size of the Mn_{16} cluster, and the resulting number of inequivalent exchange constants, it is not possible to apply the Kambe method [54] to determine the individual pairwise Mn_2 exchange interaction parameters; direct matrix diagonalization methods are also computationally unfeasible.

We concentrated instead on characterizing the spin ground state, *S*, and the zero-field splitting parameter, *D*, by performing magnetization (*M*) versus dc field measurements at applied magnetic fields and temperatures in the 1–70 kG and 1.8–10.0 K ranges, respectively. However, we could not obtain an acceptable fit using data collected over the entire field range, which is a common problem caused by low-lying excited states, especially if some have an *S* value greater than that of the ground state. A common solution to this problem is to use only data collected at smaller fields and/or lower temperatures; however, it was still not possible to get a satisfactory fit even with data below 1 T and 5 K [18,19]. This suggests that low-lying excited states are populated even at these relatively low temperatures.

Ac magnetic susceptibility studies at zero dc field and 3.5 G ac field were also carried out. In the ac susceptibility experiment, the ac magnetic field is oscillating at a particular frequency and a peak in the out-of-phase χ''_M versus *T* plot is observed when the magnetic moment of the molecule cannot relax fast enough to keep in-phase with the oscillating field. As we have described before on multiple occasions [18,19,29,38], ac susceptibility studies are also a powerful complement to dc studies for determining the ground state of a system, because they preclude any complications arising from the presence of a dc field. We thus decided to carry out ac studies on complex **1** as an independent probe of its ground state, *S*. These were performed in the 1.8–15 K range using a 3.5 G ac field oscillating at frequencies in the 50–1000 Hz range. Fig. 10 shows the in-phase component of the ac susceptibility as $\chi'_M T$ versus *T*, while the out-of-phase susceptibility, as χ''_M versus *T*, is shown in Fig. 11.

The $\chi'_M T$ product decreases almost linearly with decreasing temperature below 15 K, indicating depopulation of excited states with spin *S* larger than that of the ground state and further justifying the problematic fits of the dc magnetization data. Extrapolation of the $\chi_M T$ data from above ~6.0–0 K, where only the ground state will be populated, gives a value of ~3 $cm^3\ mol^{-1}$ K, indicative of an $S = 2$ ground state with $g = 2$. Utilizing instead

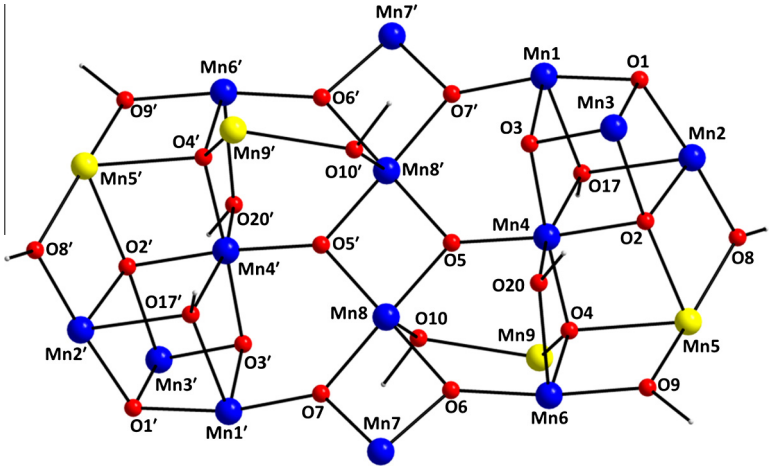

Fig. 6. Partially labeled PovRay representation of the $[Mn_{18}(\mu_4\text{-}O)_4(\mu_3\text{-}O)_{10}(\mu_3\text{-}OR)_2(\mu\text{-}OR)_8]^{12+}$ core of **4**. Color scheme: same as in Fig. 5. (Color online.)

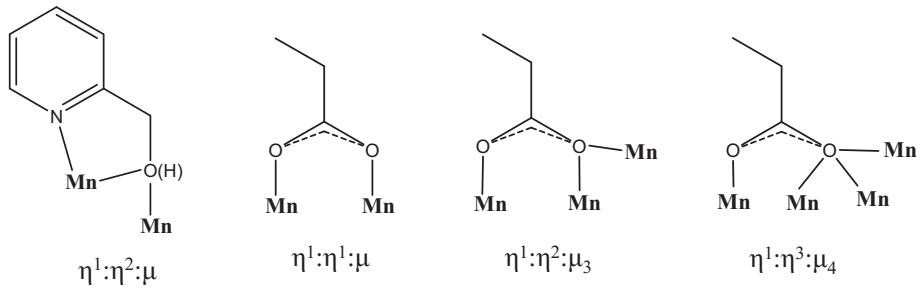

Fig. 7. The coordination modes of hmp^-/hmpH and $EtCO_2^-$ groups present in complex **4**.

Table 5
Bond valence sum (BVS)[a,b] calculations for Mn and selected O atoms in **4**.

Atom	Mn^{II}	Mn^{III}	Mn^{IV}
Mn1	3.22	2.94	3.10
Mn2	3.14	2.87	3.02
Mn3	3.21	2.93	3.08
Mn4	3.20	2.93	3.07
Mn5	2.02	1.86	1.93
Mn6	3.14	2.87	3.01
Mn7	3.22	2.94	3.09
Mn8	3.14	2.88	3.02
Mn9	1.99	1.83	1.90
Atom	BVS	Assignment	
O1	1.70	O^{2-} (μ_3)	
O2	1.76	O^{2-} (μ_4)	
O3	1.86	O^{2-} (μ_3)	
O4	1.80	O^{2-} (μ_4)	
O5	1.84	O^{2-} (μ_3)	
O6	1.83	O^{2-} (μ_3)	
O7	1.88	O^{2-} (μ_3)	

[a] The underlined value is the one closest to the charge for which it was calculated. The oxidation state is the nearest whole number to the underlined value.
[b] An O BVS in the ~1.7–2.0, ~1.0–1.2, and ~0.2–0.4 ranges is indicative of non-, single- and double-protonation, respectively.

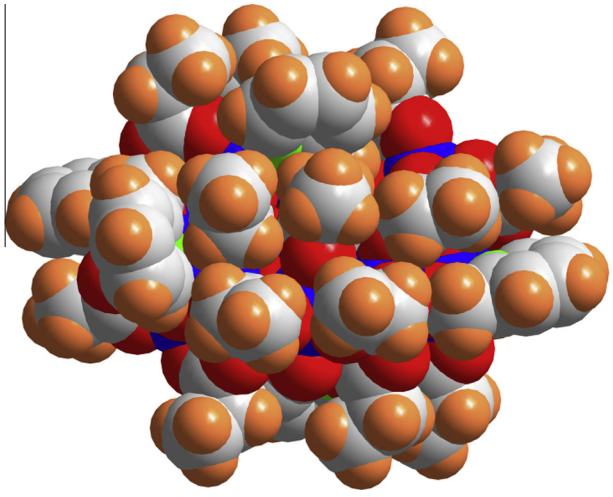

Fig. 8. Space-filling representation of **4**. Color scheme: Mn blue; O red; N green; C gray; H beige. (Color online.)

the $\chi_M'T$ data below 6 K and extrapolating them to 0 K, we get a value of ~1 $cm^3\ mol^{-1}\ K$, suggestive of an $S = 1$ ground state ($g = 2$). We thus conclude that complex **1** has either an $S = 2$ or 1 ground state, but these are nevertheless very close in energy even at the lowest possible temperatures. Finally, complex **1** does not exhibit an out-of-phase ac magnetic susceptibility signal down to 1.8 K, indicating that it is not an SMM.

3.3.2. Magnetic susceptibility studies of complex *4*

Variable-temperature dc and ac magnetic susceptibility measurements were performed on powdered polycrystalline samples of **3** and **4**, restrained in eicosane to prevent torquing, in a 1 kG (0.1 T) field and in the 5.0–300 K range. Again, the magnetic data of **3** and **4** are identical, and therefore only those of **4** (Fig. 12) will be discussed in detail.

The $\chi_M T$ product for **4** steadily decreases with decreasing temperature from 41.19 $cm^3\ mol^{-1}\ K$ at 300 K to 32.89 $cm^3\ mol^{-1}\ K$ at 100 K, then plateaus till ~40 K, before dropping further to 2.83 $cm^3\ mol^{-1}\ K$ at 5.0 K. The shape of the plot indicates predominant antiferromagnetic exchange interactions between the metal centers. The 300 K value is much less than the spin-only ($g = 2$) value of 59.5 $cm^3\ mol^{-1}\ K$ for $4Mn^{II}$ and $14Mn^{III}$ non-interacting ions, further suggesting the presence of antiferromagnetic exchange interactions within the compound. The 5 K value indicates that complex **4** possesses a small spin ground state value or even $S = 0$. An accurate determination of the ground state of **4** using *M* versus *H* data in a wide temperature and dc field range was again unfeasible due to the presence of low-lying excited states close in energy with the ground state. We have thus focused on ac susceptibility studies because they preclude any complications arising from the presence of a dc field and they can also help elucidating the magnetic dynamics of a system. To that end, extrapolation of the linearly decreasing $\chi_M'T$ data (Fig. 13) from the 2–15 K region to 0 K, where only the ground state will be populated, gives a value close to 0 $cm^3\ mol^{-1}\ K$, indicative of an $S = 0$ ground state. As expected, complex **4** did not exhibit an out-of-phase ac magnetic susceptibility signal down to 1.8 K, indicating that it is not an SMM.

4. Conclusions

We have recently focused on how the employment of cyanates in Mn cluster chemistry will lead to chemically, structurally, and magnetically new findings, distinctly different than those observed from the use of the related azido ligands. The present work extends our previous results in this area, where $Mn_{14}^{II/III}$ and $Mn_{16}^{II/III/IV}$ clusters had been obtained from the employment of cyanato groups in higher oxidation state manganese cluster chemistry [16], in conjunction with the *gem*-diolate form of di-2-pyridylketone and 2,6-diacetylpyridine dioxime, respectively. Although the reported mixed-valence Mn(II/III) cluster compounds **1**–**4** do not contain bridging cyanato groups, which was actually the main objective of this project, they have nevertheless been isolated in the presence of OCN^- ions and hmpH chelate. Furthermore, it was found that the nature

Table 6
Chemical formulae, oxidation states description, ground-state *S* values, and nature of magnetic exchange interactions for polynuclear Mn complexes with a nuclearity of 16.

Complex[a,b]	Oxidation states	*S*	Magnetic interactions	Refs.
$[Mn_{16}O_8(OH)_4Cl_2(OCN)_4(L1)_2(dapdo)_6(DMF)_4]$	$Mn^{II}_8Mn^{III}_4Mn^{IV}_4$	7	AF and F (non-SMM)	[16]
$[Mn_{16}O_4(OH)_4(L2)_8]^{4+}$	Mn^{II}_{16}	n.r.	AF (non-SMM)	[35]
$[Mn_{16}(OH)_8(L3)_8]^{8+}$	Mn^{II}_{16}	n.r.	AF (non-SMM)	[36]
$[Mn_{16}(pbshz)_{16}(DMF)_6(H_2O)_{10}]$	Mn^{III}_{16}	n.r	n.r	[37]
$[Mn_{16}(O_2CMe)_{16}(teaH)_{12}]$	$Mn^{II}_8Mn^{III}_8$	10	AF (SMM)	[38]
$[Mn_{16}(O_2CPr^i)_{16}(teaH)_{12}]$	$Mn^{II}_8Mn^{III}_8$	11	AF (SMM)	[38]
$[Mn_{16}(O_2CMe)_8(O_2CPr)_8(teaH)_{12}]$	$Mn^{II}_8Mn^{III}_8$	12	AF (SMM)	[39]
$[Mn_{16}O_{16}(OMe)_6(O_2CMe)_{16}(MeOH)_3(H_2O)_3]$	$Mn^{III}_{10}Mn^{IV}_6$	n.r.	AF (SMM)	[40]
$[Mn_{16}O_{16}(OMe)_6(O_2CCH_2Ph)_{16}(MeOH)_6]$	$Mn^{III}_{10}Mn^{IV}_6$	n.r.	AF (SMM)	[41]
$[Mn_{16}O_{16}(OMe)_6(O_2CCH_2Cl)_{16}(MeOH)_6]$	$Mn^{III}_{10}Mn^{IV}_6$	n.r.	AF (SMM)	[41]
$[Mn_{16}O_{16}(OMe)_6(O_2CCH_2Br)_{16}(MeOH)_6]$	$Mn^{III}_{10}Mn^{IV}_6$	n.r.	AF (SMM)	[41]
$[Mn_{16}O_8(O_2CPh)_{14}(mpko)_4(dpkd)_4]$	$Mn^{II}_6Mn^{III}_{10}$	3	AF (SMM)	[42]
$[Na_4Mn_{16}O_4(N_3)_{11}(OMe)_4(L4\text{-}H_2)_{12}(H_2O)_4]^+$	$Mn^{II}_4Mn^{III}_{12}$	n.r.	AF (non-SMM)	[43]
$[Mn_{16}O_8(OMe)_4(O_3PCHPh_2)_8(O_2CBu^t)_6(H_2O)(MeOH)_2(py)_2]$	$Mn^{II}_6Mn^{III}_{10}$	n.r.	AF	[44]
$[Mn_{16}O_8(OH)_2(O_2CPh)_{12}(hmp)_{10}(H_2O)_2]^{2+}$	$Mn^{II}_6Mn^{III}_{10}$	8	AF (SMM)	[45]
$[Mn_{16}O_8(OMe)_4(OCN)_4(O_2CMe)_{12}(hmp)_6(MeOH)_2]$	$Mn^{II}_6Mn^{III}_{10}$	2 or 1	AF (non-SMM)	t.w.
$[Mn_{16}O_2(OMe)_{12}(O_2CMe)_{10}(tmp)_8]$	$Mn^{II}_2Mn^{III}_{10}Mn^{IV}_4$	14 ± 1	F (SMM)	[46]

[a] Counterions and solvate molecules are omitted.
[b] *Abbreviations:* F = ferromagnetic; AF = antiferromagnetic; n.r. = not reported; t.w. = this work; L1-H_3 = pyridine dioximato acid; dapdoH_2 = 2,6-diacetylpyridine dioxime; L2-H_2 = bis(quinolin-2-ylmethylidene)pyrazine-3,6-dicarbohydrazone; L3-H_2 = bis(2-pyridylmethylene)pyridazin-2,6-dicarbahyzone; pbshzH_3 = N-3,3-diphenylpropionyl-salicylhydrazide; teaH_3 = triethanolamine; mpkoH = methyl 2-pyridyl ketone oxime; dpkdH_2 = *gem*-diol form of di-2-pyridyl ketone; L4-H_4 = 2-{[(2-hydroxy-3-methoxyphenyl)methylene]amino}-2-(hydroxymet-hyl)-1,3-propanediol; tmpH_3 = 1,1,1-tris(hydroxymethyl)propane.

Table 7
Chemical formulae, oxidation states description, ground-state *S* values, and nature of magnetic exchange interactions for polynuclear Mn complexes with a nuclearity of 18.

Complex[a,b]	Oxidation states	*S*	Magnetic interactions	Refs.
$[Mn_{18}O_{14}(edte)_6]^{2+}$	Mn^{III}_{18}	2 or 3	AF (SMM)	[47]
$[Mn_{18}O_{11}(OH)(OMe)(N_3)_{12}(tea)_3(teaH)_3(MeOH)]$	$Mn^{II}_3Mn^{III}_{15}$	21/2	F and AF (SMM)	[48]
$[Mn_{18}O_{12}(OMe)(N_3)_{12}(tea)_2(teaH)_4(MeOH)]$	$Mn^{II}_3Mn^{III}_{15}$	21/2	F and AF (SMM)	[49]
$[Mn_{16}O_8(O_3PPh)_{14}(O_2CBu^t)_{12}(H_2O)_2(py)_6]$	$Mn^{III}_{16}Mn^{IV}_2$	n.r.	AF (non-SMM)	[50]
$[Mn_{18}O_{14}(O_2CMe)_{18}(hep)_4(hepH)_2(H_2O)_2]^{2+}$	$Mn^{II}_2Mn^{III}_{16}$	13	AF (SMM)	[51]
$[Mn_{18}O_{14}(OMe)_{14}(O_2CBu^t)_8(MeOH)_6]$	$Mn^{II}_4Mn^{III}_{14}$	0 or 1	AF (non-SMM)	[52]
$[Mn_{18}O_{16}(O_2CPh)_{22}(phth)_2(H_2O)_4]^{4-}$	Mn^{III}_{18}	0	AF (non-SMM)	[53]
$[Mn_{18}O_{14}(O_2CEt)_{18}(hmp)_4(hmpH)_2(H_2O)_2]$	$Mn^{II}_4Mn^{III}_{14}$	0	AF (non-SMM)	t.w.

[a] Counterions and solvate molecules are omitted.
[b] *Abbreviations:* F = ferromagnetic; AF = antiferromagnetic; n.r. = not reported; t.w. = this work; edteH$_4$ = *N,N,N′,N′*-tetrakis(2-hydroxyethyl)ethylenediamine; teaH_3 = triethanolamine; hepH = 2-(hydroxyethyl)-pyridine; phthH_2 = phthalic acid.

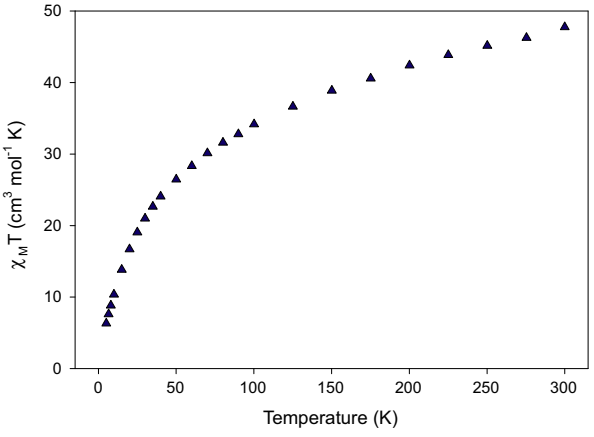

Fig. 9. $\chi_M T$ vs. *T* plot for complex **1** in a 1 kG field.

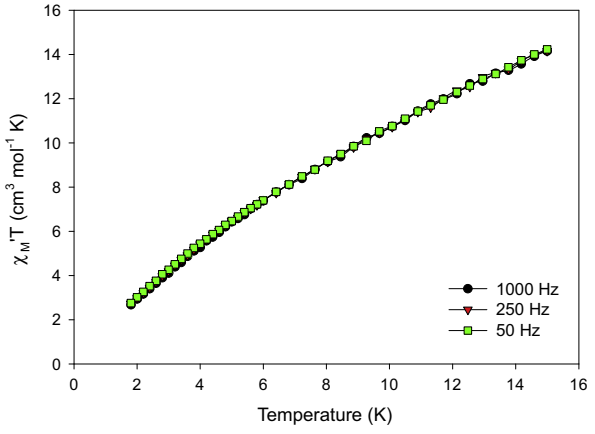

Fig. 10. Plot of the in-phase (χ'_M) signal as $\chi'_M T$ vs. *T* for complex **1** in a 3.5 G field oscillating at the indicated frequencies.

of the reaction solvent affects the identity of the isolated products; a family of Mn_{16} clusters was obtained in alcohol media while Mn_{18} compounds were crystallized in MeCN. Magnetic susceptibility studies revealed the presence of predominant antiferromagnetic exchange interactions for all complexes with small ground state spin values. It will be interesting to determine, as this work is further progressed, to what extent cyanates will continue to provide a route to new Mn clusters and to what extent these are related to clusters provided by azides.

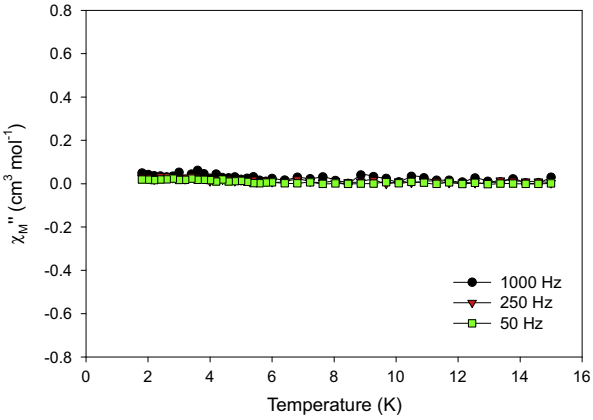

Fig. 11. Plot of the out-of-phase signal, as χ_M'' vs. T, for complex **1** in a 3.5 G field oscillating at the indicated frequencies.

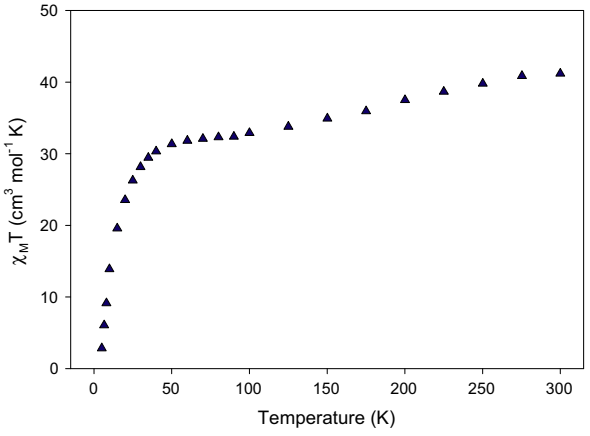

Fig. 12. $\chi_M T$ vs. T plot for complex **4** in a 1 kG field.

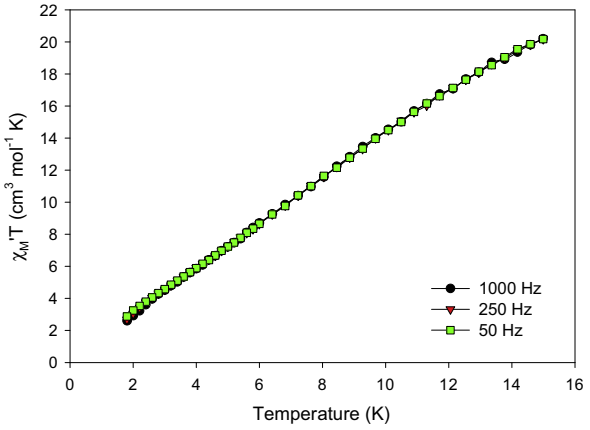

Fig. 13. Plot of the in-phase (χ_M') signal as $\chi_M' T$ vs. T for complex **4** in a 3.5 G field oscillating at the indicated frequencies.

Acknowledgements

This work was supported by Brock University, NSERC-DG and ERA (to Th.C.S), the Ontario Trillium Foundation (graduate scholarship to D.I.A), and the National Science Foundation (DMR-1213030 to G.C). The Advance Light Source is supported by The Director, Office of Science, Office of Basic Energy Sciences of the U.S. Department of Energy under contract no. DE-AC02-05CH11231.

Appendix A. Supplementary data

CCDC 1418940, 1418941, 1419572 and 1418942 contain the supplementary crystallographic data for complexes **1**–**4**. These data can be obtained free of charge via http://www.ccdc.cam.ac.uk/conts/retrieving.html, or from the Cambridge Crystallographic Data Centre, 12 Union Road, Cambridge CB2 1EZ, UK; fax: (+44) 1223-336-033; or e-mail: deposit@ccdc.cam.ac.uk.

References

[1] (a) K.N. Ferreira, T.M. Iverson, K. Maghlaoui, J. Barber, S. Iwata, Science 303 (2004) 1831;
(b) T.G. Carrell, A.M. Tyryshkin, G.C. Dismukes, J. Biol. Inorg. Chem. 7 (2002) 2;
(c) V.K. Yachandra, K. Sauer, M.P. Klein, Chem. Rev. 96 (1996) 2927;
(d) C.F. Yocum, V.L. Pecoraro, Curr. Opin. Chem. Biol. 3 (1999) 182.
[2] (a) G. Christou, D. Gatteschi, D.N. Hendrickson, R. Sessoli, MRS Bull. 25 (2000) 66;
(b) G. Aromi, E.K. Brechin, Struct. Bond. 122 (2006) 1;
(c) R. Bircher, G. Chaboussant, C. Dobe, H.U. Gudel, S.T. Ochsenbein, A. Sieber, O. Waldman, Adv. Funct. Mater. 16 (2006) 209;
(d) M. Murrie, D.J. Price, Annu. Rep. Prog. Chem. Sect. A 103 (2007) 20.
[3] D. Gatteschi, R. Sessoli, Angew. Chem., Int. Ed. 42 (2003) 268.
[4] M. del Carmen Gimenez-Lopez, F. Moro, A. La Torre, C.J. Gomez-Garcia, P.D. Brown, J. van Slageren, A.N. Khlobystov, Nat. Commun. 2 (2011) 407.
[5] R. Vincent, S. Klyatskaya, M. Ruben, W. Wernsdorfer, F. Balestro, Nature 488 (2012) 357.
[6] G. Aromí, D. Aguilà, P. Gamez, F. Luis, O. Roubeau, Chem. Soc. Rev. 41 (2012) 537.
[7] (a) For example, see: Z. Wang, J. van Tol, T. Taguchi, M.R. Daniels, G. Christou, N.S. Dalal, J. Am. Chem. Soc. 133 (2011) 17586;
(b) R.T.W. Scott, S. Parsons, M. Murugesu, W. Wernsdorfer, G. Christou, E.K. Brechin, Angew. Chem., Int. Ed. 44 (2005) 6540.
[8] (a) J. Ribas, A. Escuer, M. Monfort, R. Vicente, R. Cortes, L. Lezama, T. Rojo, Coord. Chem. Rev. 193–195 (1999) 1027;
(b) A. Escuer, G. Aromí, Eur. J. Inorg. Chem. (2006) 4721;
(c) A. Escuer, J. Esteban, S.P. Perlepes, Th.C. Stamatatos, Coord. Chem. Rev. 275 (2014) 87.
[9] Th.C. Stamatatos, K.A. Abboud, W. Wernsdorfer, G. Christou, Angew. Chem., Int. Ed. 47 (2008) 6694.
[10] A.M. Ako, I.J. Hewitt, V. Mereacre, R. Clérac, W. Wernsdorfer, C.E. Anson, A.K. Powell, Angew. Chem., Int. Ed. 45 (2006) 4926.
[11] E.E. Moushi, Th.C. Stamatatos, W. Wernsdorfer, V. Nastopoulos, G. Christou, A.J. Tasiopoulos, Inorg. Chem. 48 (2009) 5049.
[12] M. Murugesu, M. Habrych, W. Wernsdorfer, K.A. Abboud, G. Christou, J. Am. Chem. Soc. 126 (2004) 4766.
[13] X.-Y. Wang, Z.-M. Wang, S. Gao, Chem. Commun. (2008) 281.
[14] (a) A.K. Boudalis, B. Donnadieu, V. Nastopoulos, J.M. Clemente-Juan, A. Mari, Y. Sanakis, J.-P. Tuchagues, S.P. Perlepes, Angew. Chem., Int. Ed. 43 (2004) 3912;
(b) G.S. Papaefstathiou, S.P. Perlepes, A. Escuer, R. Vicente, M. Font-Bardia, X. Solans, Angew. Chem., Int. Ed. 40 (2001) 884;
(c) G.S. Papaefstathiou, A. Escuer, R. Vicente, M. Font-Bardia, X. Solans, S.P. Perlepes, Chem. Commun. (2001) 2414.
[15] (a) S.M.J. Aubin, M.W. Wemple, D.M. Adams, H.-L. Tsai, G. Christou, D.N. Hendrickson, J. Am. Chem. Soc. 118 (1996) 7746;
(b) P.L. Feng, C.J. Stephenson, A. Amjad, G. Ogawa, E. del Barco, D.N. Hendrickson, Inorg. Chem. 49 (2010) 1304.
[16] D.I. Alexandropoulos, C. Papatriantafyllopoulou, C. Li, L. Cunha-Silva, M.J. Manos, A.J. Tasiopoulos, W. Wernsdorfer, G. Christou, Th.C. Stamatatos, Eur. J. Inorg. Chem. (2013) 2286.
[17] (a) N.C. Harden, M.A. Bolcar, W. Wernsdorfer, K.A. Abboud, W.E. Streib, G. Christou, Inorg. Chem. 42 (2003) 7067;
(b) E.-C. Yang, N. Harden, W. Wernsdorfer, L. Zakharov, E.K. Brechin, A.L. Rheingold, G. Christou, D.N. Hendrickson, Polyhedron 22 (2003) 1857;
(c) C. Boskovic, E.K. Brechin, W.E. Streib, K. Folting, J.C. Bollinger, D.N. Hendrickson, G. Christou, J. Am. Chem. Soc. 124 (2002) 3725;
(d) L. Lecren, O. Roubeau, C. Coulon, Y.-G. Li, X.F.L. Goff, W. Wernsdorfer, H. Miyasaka, R. Clérac, J. Am. Chem. Soc. 127 (2005) 17353;
(e) L. Lecren, W. Wernsdorfer, Y.-G. Li, O. Roubeau, H. Miyasaka, R. Clérac, J. Am. Chem. Soc. 127 (2005) 11311.
[18] Th.C. Stamatatos, K.A. Abboud, W. Wernsdorfer, G. Christou, Angew. Chem., Int. Ed. 46 (2007) 884.
[19] Th.C. Stamatatos, K.A. Abboud, W. Wernsdorfer, G. Christou, Angew. Chem., Int. Ed. 45 (2006) 4134.
[20] G. Aromí, S. Bhaduri, P. Artús, J.C. Huffman, D.N. Hendrickson, G. Christou, Polyhedron 21 (2002) 1779.
[21] G.A. Bain, J.F. Berry, J. Chem. Educ. 85 (2008) 532.
[22] Oxford diffraction. CrysAlis CCD and CrysAlis RED, Oxford Diffraction Ltd., Abingdon, Oxford, England, 2008
[23] M.C. Burla, R. Caliandro, M. Camalli, B. Carrozzini, G.L. Cascarano, L. De Caro, C. Giacovazzo, G. Polidori, R.J. Spagna, Appl. Crystallogr. 38 (2005) 381.
[24] G.M. Sheldrick, Acta Crystallogr. A64 (2008) 112.

[25] L.J. Farrugia, J. Appl. Crystallogr. 32 (1999) 837.
[26] K. Brandenburg, DIAMOND, Version 2003.2001d, Crystal Impact GbR, Bonn, Germany, 2006.
[27] A.L. Spek, J. Appl. Crystallogr. 36 (2003) 7.
[28] Bruker AXS Inc., Madison, WI, 2003.
[29] Th.C. Stamatatos, G. Christou, Inorg. Chem. 42 (2009) 3308.
[30] P.S. Perlepe, A.A. Athanasopoulou, K.I. Alexopoulou, C.P. Raptopoulou, V. Psycharis, A. Escuer, S.P. Perlepes, Th.C. Stamatatos, Dalton Trans. 43 (2014) 16605.
[31] G.B. Deacon, R.J. Phillips, Coord. Chem. Rev. 33 (1980) 227.
[32] (a) K. Nakamoto, Infrared and Raman Spectra of Inorganic and Coordination Compounds, sixth ed., Wiley, New Jersey, 2009. p. 126–128;
(b) Z. Mahendrasinh, S. Ankita, S.B. Kumar, A. Escuer, E. Suresh, Inorg. Chim. Acta 357 (2011) 333;
(c) C.R. Clough, P. Müller, C.C. Cummins, Dalton Trans. (2008) 4458.
[33] (a) W. Liu, H.H. Thorp, Inorg. Chem. 32 (1993) 4102;
(b) I.D. Brown, D. Altermatt, Acta Crystallogr., Sect. B (1985) 244.
[34] (a) V. Mereacre, A.M. Ako, R. Clérac, W. Wernsdorfer, I.J. Hewitt, C.E. Anson, A. K. Powell, Chem. Eur. J. 14 (2008) 3577;
(b) D. Dermitzaki, G. Lorusso, C.P. Raptopoulou, V. Psycharis, A. Escuer, M. Evangelisti, S.P. Perlepes, Th.C. Stamatatos, Inorg. Chem. 52 (2013) 10235.
[35] L.N. Dawe, K.V. Shuvaev, L.K. Thompson, Inorg. Chem. 48 (2009) 3323.
[36] S.K. Dey, L.K. Thompson, L.N. Dave, Chem. Commun. 47 (2006) 4967.
[37] W. Liu, K. Lee, M. Park, R.P. John, D. Moon, Y. Zou, X. Liu, H.-C. Ri, G.H. Kim, M.S. Lah, Inorg. Chem. 47 (2008) 8807.
[38] M. Murugesu, W. Wernsdorfer, K.A. Abboud, G. Christou, Angew. Chem., Int. Ed. 44 (2005) 892.
[39] S.J. Shah, C.M. Ramsey, K.J. Heroux, J.R. O'Brien, A.G. DiPasquale, A.L. Rheingold, E. del Barco, D.N. Hendrickson, Inorg. Chem. 47 (2008) 6245.
[40] D.J. Price, S.R. Batten, B. Moubaraki, K.S. Murray, Chem. Commun. (2002) 762.
[41] P. King, W. Wernsdorfer, K.A. Abboud, G. Christou, Inorg. Chem. 43 (2004) 7315.
[42] H.-S. Wang, Z.-C. Zhang, X.-J. Song, J.-W. Zhang, H.-B. Zhou, J. Wang, Y. Song, X.-Z. You, Dalton Trans. 40 (2011) 2703.
[43] D. Liu, Q. Zhou, Y. Chen, F. Yang, Y. Yu, Z. Shi, S. Feng, Dalton Trans. 39 (2010) 5504.
[44] S. Konar, A. Clearfield, Inorg. Chem. 47 (2008) 3489.
[45] T. Taguchi, W. Wernsdorfer, K.A. Abboud, G. Christou, Inorg. Chem. 49 (2010) 10579.
[46] M. Manoli, A. Prescimone, R. Bagai, A. Mishra, M. Murugesu, S. Parsons, W. Wernsdorfer, G. Christou, E.K. Brechin, Inorg. Chem. 46 (2007) 6968.
[47] A.-J. Zhou, J.-D. Leng, J.-S. Hu, M.-L. Tong, Dalton Trans. 42 (2013) 9428.
[48] Th.C. Stamatatos, D. Foguet-Albiol, W. Wernsdorfer, K.A. Abboud, G. Christou, Chem. Commun. 47 (2011) 274.
[49] S.K. Langley, K.J. Berry, B. Moubaraki, K.S. Murray, Dalton Trans. (2009) 973.
[50] M. Shanmugam, G. Chastanet, T. Mallah, R. Sessoli, S.J. Teat, G.A. Timco, R.E.P. Winpenny, Chem. Eur. J. 12 (2006) 8777.
[51] (a) E.K. Brechin, C. Boskovic, W. Wernsdorfer, J. Yoo, A. Yamaguchi, E.C. Sañudo, T.R. Concolino, A.L. Rheingold, H. Ishimoto, D.N. Hendrickson, G. Christou, J. Am. Chem. Soc. 124 (2002) 9710;
(b) E.K. Brechin, E.C. Sanudo, W. Wernsdorfer, C. Boskovic, J. Yoo, D.N. Hendrickson, A. Yamaguchi, H. Ishimoto, T.E. Concolino, A.L. Rheingold, G. Christou, Inorg. Chem. 44 (2005) 502.
[52] E.K. Brechin, W. Clegg, M. Murrie, S. Parsons, S.J. Teat, R.E.P. Winpenny, J. Am. Chem. Soc. 120 (1998) 7365.
[53] R.C. Squire, S.M.J. Aubin, K. Folting, W.E. Streib, D.N. Hendrickson, G. Christou, Angew. Chem., Int. Ed. 34 (1995) 887.
[54] K. Kambe, J. Phys. Soc. Jpn. 5 (1950) 48.